A novel approach for construction of radiocarbon-based chronologies for speleothems

Franziska A. Lechleitner[(1)*], Jens Fohlmeister[(2)], Cameron McIntyre[(1,3)], Lisa M. Baldini[(4)], Robert A. Jamieson[(4)], Helena Hercman[(5)], Michał Gąsiorowski[(5)], Jacek Pawlak[(5)], Krzysztof Stefaniak[(6)], Paweł Socha[(6)], Timothy I. Eglinton[(1)], and James U.L. Baldini[(4)]

(1) Department of Earth Sciences, ETH Zurich, Sonneggstrasse 5, 8092 Zurich, Switzerland
(2) Institute of Environmental Physics, University of Heidelberg, Im Neuenheimer Feld 229, 69129 Heidelberg, Germany
(3) Laboratory of Ion Beam Physics, ETH Zurich, Switzerland
(4) Department of Earth Sciences, Durham University, Durham, DH1 3LE, UK
(5) Institute of Geological Sciences, Polish Academy of Sciences (P.A.S.), ul. Twarda 51/55, 00-818 Warszawa, Poland
(6) Department of Palaeozoology, University of Wrocław, Sienkiewicza 21, 50-335 Wrocław, Poland

*corresponding author: franziska.lechleitner@erdw.ethz.ch

Abstract

Robust chronologies are crucial for the correct interpretation of climate proxy records and for detailed reconstructions of palaeoclimate. Stalagmites have garnered strong interest as recorders of past climate in part due to their amenability to U-series dating. However, many stalagmites are not dateable using this technique due to low ^{238}U and/or high detrital Th concentrations (e.g., many tropical cave systems (Adkins et al., 2013)), and occasionally these issues affect stalagmites across wide geographical regions (e.g., large parts of Australia (Green et al. 2013)) complicating the use of stalagmites in these areas. Radiocarbon (^{14}C) offers an alternative method of dating stalagmites, but issues associated with the 'dead carbon fraction' (DCF) have historically hindered this approach. Here, a novel ^{14}C-based method for dating stalagmites is presented and discussed. The technique calculates a best-fit growth rate between a time-series of stalagmite ^{14}C data and known atmospheric ^{14}C variability. The new method produces excellent results for stalagmites that satisfy four requirements: *i)* the absence of long-term secular variability in DCF (i.e.,

stalagmite DCF varies around a mean value with no long-term trend), *ii)* stalagmite growth rate does not vary significantly (the technique identifies stalagmites with substantial growth rate variability), *iii)* the stalagmite record is long enough that measurable ^{14}C decay has occurred, and *iv)* one 'anchor' point exists where the calendar age is known. The model produces good results for a previously U-Th dated stalagmite from Heshang Cave, China, and is then applied to an undated stalagmite from southern Poland. The new method will not replace high-precision U-Th measurements, because the precision of the technique is difficult to quantify. However, it provides a means for dating certain stalagmites undateable by conventional U-Th methods and for refining coarse U-Th chronologies.

1.Introduction

Stalagmites are becoming increasingly important climate archives, and have yielded numerous iconic records of past terrestrial climate (e.g., Cheng et al., 2009; Wang et al., 2001; Fairchild et al., 2006). Generally, stalagmites are amenable to very precise absolute dating using the U-Th method (Cheng et al., 2013; Dorale et al., 2007). The distinctly different behavior of U and Th in drip waters means that stalagmite carbonate theoretically contains almost no ^{230}Th when deposited, and that subsequent ^{230}Th accumulation results purely from radioactive decay of ^{238}U and ^{234}U, allowing precise determination of carbonate precipitation age (van Calsteren and Thomas, 2006). Additionally, the development of powerful analytical techniques, initially Thermal Ionisation Mass Spectrometry (TIMS) (Edwards et al., 1987; Li et al., 1989) and subsequently Multi-Collector Inductively Coupled Plasma Mass Spectrometery (MC-ICPMS) (Hoffmann et al., 2007), have greatly improved chronological precision. However, stalagmites either with high detrital Th (not derived from in situ radioactive decay) or with extremely low uranium concentrations have proven problematic, and are occasionally not dateable using this approach (González-Lemos et al., 2015; Urban et al., 2015). Young stalagmites (< 300 years), where the U-Th method has its largest uncertainties, are most susceptible to these issues (Hodge et al., 2011; Mattey et al., 2008).

The first method proposed to develop chronologies for stalagmite-based climate records was ^{14}C dating (Broecker et al., 1960; Hendy and Wilson, 1968), due to its already widespread application to other terrestrial archives such as tree rings and lake sediments (e.g., Reimer et al., 2013; Street and Grove, 1979; Suess, 1980) and in groundwater research (Wigley, 1975). However, ^{14}C in groundwater and consequently stalagmite carbonate reflects contemporaneous atmospheric ^{14}C combined with variable amounts of ^{14}C-depleted carbon from the soil and host rock. This reservoir effect, termed the "dead carbon fraction" (DCF, used hereafter in this text), or "dead carbon proportion" (dcp, DCP), if not properly constrained, results in stalagmite ages that are too old (Genty and Massault, 1999; Genty et al., 2001; Holmgren et al., 1994). Formally, DCF is expressed as:

$$DCF = 1 - \left(a^{14}C_{stal.init.} \Big/ a^{14}C_{atm.init.} \right) \quad (1)$$

where $a^{14}C_{stal.\,init.}$ and $a^{14}C_{atm.\,init.}$ represent stalagmite and atmosphere ^{14}C activity (respectively) at the time of carbonate deposition. Potentially unquantifiable DCF variability, combined with contemporaneous analytical advances involving the U-Th method, resulted in the dismissal of ^{14}C-dating of stalagmites as a viable approach (Gascoyne, 1992; Genty et al., 2001). The issues with absolute ^{14}C dating of stalagmites revolve around accurate quantification of DCF. Solving this problem would thus open the door to the application of the technique to speleothems. Over the past two decades, numerous studies have attempted to identify mechanisms governing DCF and its variability, largely with the aim of using DCF as tracer for hydrological and carbon cycle processes (Fohlmeister et al., 2011, 2010; Genty and Massault, 1999; Genty et al., 2001; Griffiths et al., 2012; Noronha et al., 2014). This past research strongly suggests that host rock dissolution processes and the degree of open- versus closed-system behavior within the karst (Fohlmeister et al., 2010; Griffiths et al., 2012; Noronha et al., 2014), as well as contributions from soil organic matter (Oster et al., 2010; Scholz et al., 2012), exert primary control on DCF variability. All these processes are dependent on hydrological conditions, and consequently several recent papers have proposed that changes in DCF reflect past hydroclimate variability (Griffiths et al., 2012; Noronha et al., 2014; Oster et al., 2010). Additionally, the

location of the atmospheric 'bomb spike' (resulting from widespread nuclear testing in the 1950s and 1960s) within stalagmite stratigraphy represents a potentially useful chronological tool. For example, Mattey et al. (2008) and Hodge et al. (2011) used the bomb spike imprint to date stalagmites by inverse modelling of their ^{14}C uptake, providing a method for development of robust chronologies for very recent deposits (~1950-present) where U-Th techniques are less precise. Hua et al. (2012) constructed additional chronologies for two of the stalagmites used by Hodge et al. (2011) using the ^{14}C bomb spike combined with high-resolution $\delta^{18}O$ and $\delta^{13}C$ measurements. Another approach is illustrated in González-Lemos et al. (2015), who used $\delta^{13}C$ values to define periods of similar DCF, assuming a comparable hydrological influence on both parameters. These studies have applied ^{14}C dating to stalagmites using very different approaches to constrain DCF, illustrating the potential applicability of the technique to stalagmites. For most samples, U-Th dating produces the best dates, but for samples not amenable to U-Th dating, the ^{14}C method provides an alternate chronological tool. Additionally, high precision ^{14}C dating typically requires only 8-10 mg powered sample, compared to up to several 100 mg for U-Th, which is advantageous in many situations.

Here we present a new method for the construction of accurate stalagmite chronologies using ^{14}C. The method determines the mean stalagmite growth rate by comparing a long stalagmite ^{14}C time-series to atmospheric ^{14}C over the same time interval. The technique is not yet applicable to all stalagmites, but highlights promising aspects of stalagmite ^{14}C records that could be refined to fit a wide variety of samples.

2.Sample description

Stalagmite NIED08-05 was collected in 2008 from Niedźwiedzia Cave in Kletno, Poland (Fig. 1). The cave has been a closed system since the Early Holocene, with access to the surface only through ponors (Don, 1989; Pflitsch and Piasecki, 2003). However, the presence of cave bear skulls and entire skeletons in the cave indicate that there must always have been a relatively large opening to the outside world (Bieronski et al., 2009). The first 200 m of cave passage were

discovered in 1966 during marble mining followed by an additional ~2 km in 1982.

The cave's isolation from the outside atmosphere would have minimized external influences, and encouraged slow calcite growth. NIED08-05 grew in the upper level of Niedźwiedzia Cave, approximately 10 meters below the surface (Fig. 1), where air temperature is very stable (<1.0°C variation around the multi-annual average), and relative humidity (RH) is almost 100% (Piasecki and Sawinski, 2009). The mean annual temperature within the cave is 6˚C, reflecting the mean annual outside temperature. To ensure active stalagmite growth, the drip feeding NIED08-05 was monitored for ~three months (04 April - 20 June 2008) using a Stalagmate drip counter. After removal from the cave, NIED08-05 was sectioned along its growth axis and polished at Durham University. The stalagmite is 12.5 cm long and composed of very dense, coarse crystalline calcite (Fig. 2a). No regular visible laminae exist, except for a few white microcrystalline layers that may reflect growth hiatuses. Very low concentrations of ^{238}U (mean concentrations = ~14 ppb) prevented high-precision U-Th dating, as typical dating errors over the Holocene were between 190 and 4065 years, with numerous stratigraphic inversions. Because the stalagmite was otherwise an excellent sample (free from detrital contamination, appropriate crystal morphology, from a region with few long palaeoclimate records), it was decided to date the sample using ^{14}C.

3.Analytical methods

3.1. ^{14}C measurements

Samples for high-precision graphite ^{14}C analysis were drilled at 5 mm resolution along the growth axis using a semi-automatic high precision drill (Sherline 5400 Deluxe) at ETH Zurich. To minimise potential contamination, all the equipment and the stalagmite were cleaned with methanol and dried using compressed air prior to sampling, and the top 0.1 mm of stalagmite surface powder was discarded. Aliquots of ~8 mg of carbonate powder were dissolved in 1 ml of 85% H_3PO_4. Fast carbonate dissolution and a complete conversion to CO_2 were ensured by heating the sample vials to 85°C for one hour. Graphitisation was performed using an Automatic Graphitization Equipment (AGE) system (Wacker

et al., 2010) via iron-catalysed hydrogen reduction of the CO_2. The resultant graphite was transferred to aluminum targets for determination of ^{14}C activities ($a^{14}C$) using a Mini radioCarbon Dating System (MICADAS) accelerator mass spectrometer (AMS) (Synal et al., 2007) at the Laboratory for Ion Beam Physics (LIP) at ETH Zurich. In addition, detailed sampling and ^{14}C analysis was undertaken to detect the atmospheric ^{14}C bomb spike imprint. For this, the top 1mm of NIED08-05 was milled at an extremely high resolution (100µm per sample) over four different tracks. Approximately 0.8 mg of carbonate were dissolved in 85% H_3PO_4, and the CO_2 produced was measured directly on the MICADAS using a Gas Ion Source (GIS) system (Ruff et al., 2007), again at LIP. A series of laboratory standards (Oxalic acid II, IAEA C1 and C2, and a modern coral standard) were used to ensure high precision: Oxalic acid II was measured to a precision of better than 2‰ for graphite and 10‰ for GIS analyses. In addition, ^{14}C-dead stalagmite material (stalagmite material from NE India, MAW-1: ~170 kyr, based on U-Th dates) was used as a procedural blank during all measurement runs.

3.2 Stable isotope and trace element analysis

260 samples for stable isotope analysis were milled continuously along the growth axis, using a Proxxon micromill at Durham University. The samples were transferred to glass Exetainer vials and flushed with He to remove outside air before acid digestion using 103% H_3PO_4. The measurement was conducted on a Thermo-Finnigan MAT253 Isotope Ratio Mass Spectrometer at Durham University, and uncertainties were assessed from standards NBS-18, NBS-19, LSVEC and an in-house standard. External analytical uncertainties for both $\delta^{13}C$ and $\delta^{18}O$ are 0.1‰ and presented relative to the Vienna Pee Dee Belemnite (V-PDB).

A high-resolution profile of major trace elements over the top ca. 105 mm of NIED08-05 was produced using a prototype RESOlution M-50 excimer (193 nm) laser-ablation system with a two-volume laser-ablation cell coupled to an Agilent 7500ce/cs quadrupole ICPMS at Royal Holloway University, London. Müller et al. (2009) describe in detail the analytical configuration and initial performance

metrics. The profile was measured using a 140 by 10µm rectangular laser slit, a 15Hz repetition rate of a 90mJ laser spot, and a 10µm s^{-1} scan speed. Samples were bracketed by analyses of NIST 612, NIST 610 and MACS3 standards for quantification. Data reduction was performed using the Iolite software package using NIST 610/612 standards for external standardization (Paton et al., 2011). Calcium-43 was measured throughout the sample runs as an internal standard.

4.Results

4.1.^{14}C measurements: chronology and bomb spike identification

Twenty-five high-precision graphite ^{14}C ages, ranging from 1,139±27 years at 5 mm from the top to 8,909±38 years at the base (122 mm from the top), were all in stratigraphic order within measurement uncertainty, apart from a small reversal at 102 mm depth (Fig. 2a, Table 1). The ^{14}C data suggest the NIED08-05 growth spans much of the Holocene, in agreement with the initial assumption based on the very imprecise U-Th ages. Very regularly increasing ^{14}C ages with depth suggest generally constant stalagmite growth. However, an abrupt 1,700-year shift occurs between 47 and 52 mm from top coinciding with a thin white microcrystalline layer, strongly suggesting the presence of a growth hiatus (Fig. 2a). Similar microcrystalline layers elsewhere in the stalagmite suggest that other hiatuses exist, but because the ^{14}C ages do not indicate growth interruption at these times these possible (probably very brief) hiatuses were not considered in the final chronology. The very high resolution GIS measurements along the top 1 mm of NIED08-05 show considerably increased ^{14}C activity in the uppermost 0.4 mm in three out of four replicate tracks, confirming the presence of the bomb spike (Fig. 2b, Suppl. Table 1). The different manifestations of the atmospheric ^{14}C bomb spike in the four traverses is attributable to strong signal attenuation in the karst (max. a^{14}C = 0.96 fraction modern (fM) compared with 1.98 fM in the atmosphere in 1963; Hua et al., 2013), to sampling bias due to the transect position relative to stalagmite curvature, and to the remarkably high-resolution nature of these ^{14}C analyses. All samples were larger than the threshold where significant blank contributions occur that could influence the reliability of the results (see section **Error! Reference source not found.**). To our knowledge,

these are the first high-resolution ^{14}C measurements performed on replicate tracks in a stalagmite.

Replicate blank measurements on milled aliquots of the ^{14}C-dead stalagmite MAW-1 ensure that no contamination from modern atmospheric ^{14}C during carbonate drilling, as encountered by previous studies (Hoffmann et al., 2010; Southon et al., 2012), occurred.

4.2. Stable isotope and trace element analysis

Overall, in NIED08-05 $\delta^{13}C$ remains very stationary with only a minor longer-term trend (mean = -7.48‰, σ = 1.17, Suppl. Fig. 1). Conversely, Mg concentrations are quite variable throughout the stalagmite (mean Mg/Ca ratio x 1000 = 2.56, σ = 0.85). Several large excursions exist within the Mg dataset, with gradual increases in Mg/Ca followed by more abrupt decreases (e.g. at 10 mm, 44 mm and 51.5 mm from top) possibly reflecting karst hydrology processes and/or growth hiatuses (Suppl. Fig. 1).

5.Chronology development

The technique described herein does not utilise ^{14}C ages as discrete dates, but instead focusses on the topology of the long-term $a^{14}C$-depth relationship. Regularly decreasing $a^{14}C$ with depth from the sample top strongly suggests that only small stalagmite growth rate and DCF changes occurred, and that exponentially decreasing $a^{14}C$ is only due to radioactive decay. In this case, the best-fit line describing the ^{14}C data should reflect the stalagmite's long-term average growth rate, and a simple chronology can be built by anchoring the growth rate to a point of known age (such as collection date, or the bomb spike). Similar approaches are used in other fields of geochronology, for example in ^{210}Pb dating of sediments over the last 100 years (Appleby & Oldfield, 1978; Baskaran et al., 2014) or in ^{230}Th excess dating of deep sea sediments (Francois et al., 1990). However, whereas those methods generally assume that radionuclide incorporation rate is essentially constant over time, this is not the case with ^{14}C due to past variations in atmospheric $a^{14}C$ (e.g., Reimer et al., 2013).

The model presented here identifies stalagmites with 'stationary' growth rates over long time intervals (i.e., samples with growth rates that vary around a long-term mean value). Stationarity in DCF implies that no secular changes in both the soil organic matter age and the host rock dissolution systems (open vs. closed) occurred. Secular changes in DCF define long-term trends resulting from large fluctuations in climate (e.g. deglaciations (Rudzka et al., 2011)) or changes in the cave's carbon cycle (e.g. build-up of soils (Genty et al., 2001; Scholz et al., 2012)). These trends in DCF are detectable using through other geochemical proxies, such as $\delta^{13}C$ and Mg/Ca, as demonstrated by many previous studies (e.g. Scholz et al., 2012, Genty et al., 2001, Rudzka et al., 2011). Such long-term changes in DCF would preclude a stalagmite to be suitable for the method presented here. Small DCF variations around a long-term mean value, however, are permissible.

Assuming that the stationarity condition is met, the model builds an age-depth relationship accounting for both variable DCF and atmospheric ^{14}C. There are two principal steps to the process: *i*) the chronology is anchored to an independent point of known age and *ii*) an iterative, MATLAB-based process adjusts modelled stalagmite growth rate by considering past atmospheric a^{14}C variability. If DCF remains stationary on long timescales, short-term (seasonal or longer term) DCF fluctuations around a mean value do not affect the calculations. This is not dissimilar to U-Th dating, which only produces ages for a few select depths and infers the ages of other depths (and consequently growth rates) using best-fit equations.

5.1.Model setup

The model is based on the radioactive decay equation, expressed by:

$$A/A_0 = e^{-\lambda t} \quad (2)$$

where A is the ^{14}C activity measured in the stalagmite, A_0 is the initial stalagmite ^{14}C activity, and λ is the ^{14}C decay constant (1/8267 yr^{-1}). Carbonate deposition age (t) is unknown and is expressed as:

$$t = {}^{d}/_{R} \quad (3)$$

where d is the depth from the stalagmite top and R is the growth rate.

Converting equation 2 to its linear form with respect to t yields:

$$\ln\left({}^{A}/_{A_0}\right) = -\lambda t \quad (1)$$

and if

$$\ln\left({}^{A}/_{A_0}\right) = -\lambda + {}^{d}/_{R} \quad (2)$$

the slope is proportional to $1/R$.

Variable atmospheric ^{14}C and karst carbon transfer dynamics (i.e., DCF) complicate quantifying A_0. A point of known age anchors the entire chronology taking into account DCF, and thus atmospheric $a^{14}C$ entirely drives A_0.

5.2. Anchor point selection and identifying the best-fit decay curve

The model requires a point of known age to account for DCF, and therefore the 'anchor point' needs to be defined before starting the modelling procedure. For stalagmites that were growing when collected, the collection date is suitable. Other possibilities are the beginning of the bomb spike rise (i.e., the first indication of bomb ^{14}C in the atmosphere, 1955 AD), or a robust U-Th measurement, if available. In the first step, the model computes a best fit through all $a^{14}C$ measurements in the dataset, defining an initial growth rate (Fig. 3a). A_0 is kept at 1 for this step (i.e., constant atmospheric ^{14}C). The anchor point permits calculation of each sample's calendar age via the growth rate. Because A_0 = 1, this initial age-depth relationship requires further refinement. In the second iteration, atmospheric ^{14}C values from the IntCal13 calibration curve (Reimer et al., 2013), corresponding to the calculated sample ages, are assigned as new A_0 values and a new, slightly different growth rate is calculated. Atmospheric ^{14}C values from the IntCal13 are smoothed prior to the fitting procedure using a moving average (window size 5) to mimic the effect of soil organic matter and

vegetation on the soil CO_2 (Fohlmeister et al., 2011). The stalagmite ages are then re-adjusted accordingly, with a static anchor point (i.e., unchanged from iteration 1). The procedure is repeated until convergence is reached and growth rate changes become insignificant (<0.0001mm yr^{-1}). This condition is typically reached after four to six iterations of the fitting procedure (Fig. 3).

5.3. Hiatus integration in the model

Constraining and delimiting the duration and exact timing of hiatuses is critical for developing accurate chronologies. The probable lack of an anchor point below hiatuses complicates applying the model described here, as is the case in NIED08-05 for the growth interval older than the depositional hiatus ('pre-hiatus'). A modified version of the method can develop the pre-hiatus chronology, although only qualitatively.

For stalagmites with a depositional hiatus, the model initially constrains the post-hiatus interval as in section 5.2., permitting the calculation of mean DCF for that interval. Assuming stationary DCF over the entire stalagmite, this mean DCF and its standard deviation are applied to all ^{14}C ages from the pre-hiatus interval. The DCF corrected ^{14}C ages are then calibrated to calendar years using a procedure similar to commonly available calibration tools, but built into the MATLAB modelling procedure. Correcting and calibrating all pre-hiatus ages prevents over- or under-estimation of the stalagmite age due to a single offset age (from a possible extreme DCF value), and is therefore more robust than treating only one individual (i.e., the first) pre-hiatus age. The calibration of the DCF corrected ^{14}C ages provides a probability density distribution in time for each ^{14}C age. The best growth rate (Fig. 3b, red line) through the probability densities of all ages is determined by using the following procedure: *i)* the youngest pre-hiatus age acts as a preliminary anchor point, and the constant growth rate line is positioned through that point (Fig. 3b, red line); *ii)* The growth rate line is then shifted gradually through time, intersecting each point of the calibrated age probability distribution at a certain point (Fig. 3b); *iii)* The probabilities of the intersection points are added and quantify the constant growth rate line's fit to the entire data (Fig. 3c). *iv)* Shifting the line of constant

364 growth through the calibrated ^{14}C ages establishes a new probability function for
365 the placement of this line. The best placement is determined using the weighted
366 mean of the probability distribution, which again ensures that the model is not
367 biased by single offset ages (Fig. 3c).
368
369 5.4.Uncertainties and error estimation
370 The model considers different sources of error, including: A) Estimated growth
371 rate error, related to the goodness of the fit through the measured ^{14}C data; B)
372 Measurement error regarding the depth from stalagmite top (i.e. uncertainty
373 introduced from the sampling); C) Error on the calculated mean DCF, defined by
374 its standard deviation, and D) Uncertainty from the calibration, given by the
375 probability density distribution of the calibrated ^{14}C ages.
376
377 For the simple case of an age model without any hiatus, the resulting uncertainty
378 depends only on errors of type A and B. The chronological uncertainty is
379 calculated using common error propagation, and increases with distance from
380 the anchor point, due to uncertainty in the growth rate estimate (uncertainty in
381 the slope determined during the fitting procedure). In this case, the model's
382 chronological error is small, and depends on how well the anchor point is
383 constrained. If a hiatus is present, the chronological uncertainty for the lower
384 part is assessed differently, and the uncertainty is governed largely by type C and
385 D errors, whereas other errors are trivial and not considered. Because the age
386 model's pre-hiatus interval is not based on a single anchor point, but rather all
387 ^{14}C ages act as anchor points, the uncertainty is defined by the new probability
388 function for the placement of the constant growth rate line (Fig. 3c). This results
389 in much larger errors than for the case with no hiatus.
390
391 6.Model testing and application
392 6.1.Stalagmite HS4 (Heshang Cave)
393 The model was tested using a previously published stalagmite ^{14}C dataset from
394 Heshang Cave (China) (Noronha et al., 2014). Stalagmite HS4 is 250 cm tall and
395 was dated using U-Th techniques, which suggest continuous growth with an
396 almost constant growth rate over the past ~8,000 years (Hu et al., 2008). DCF is

stationary but varied between 7 and 14% (Noronha et al., 2014); therefore the sample is ideal for testing the reliability of the ^{14}C chronology development technique presented here.

The exponential decay function was transformed to a linear relationship to simplify data visualization and handling. Removing the linear trend from the natural logarithm of the $a^{14}C$ ('ln ($a^{14}C$)') data reveals that the top three ^{14}C ages in HS4 are anomalous (defined as ages more than 1σ away from the dataset's mean (Suppl. Fig. 2)), possibly due to a shift in growth rate or DCF. If a growth rate shift occurred, and an anchor point were chosen in the anomalous interval, an offset in the age-depth model may result. To avoid chronological bias, the anchor was therefore set to the first ^{14}C data point beyond the anomalous top interval (the fourth ^{14}C point from the top overall) (Suppl. Fig. 2), rather than at the first data point from the top of the ^{14}C dataset. Growth rate convergence was reached after four iterations, and comparison between modelled and actual growth rate (derived from U-Th dating) show excellent agreement (modelled ^{14}C growth rate = 0.0262 ±0.00047 cm yr^{-1}; U-Th growth rate = 0.0259 cm yr^{-1}). The model's chronological error is between ±1 and ±155 years (Fig. 4). In comparison, if the first data point from the top of the ^{14}C dataset is used as anchor point, the modelled ages are overestimated throughout most of the chronology. Consequently DCF is underestimated on average by 3% (max. underestimation = 6%), although the chronological precision is unchanged (Fig. 4). A shortcoming of the model is therefore its dependency on the choice of anchor point; even with prolonged, nearly constant growth rate, the anchor point determines chronological accuracy. A detailed analysis of the raw ^{14}C data profile can help evaluating the suitability of any chosen anchor point, and assessment of whether that point is representative of average DCF throughout the stalagmite.

6.2.NIED08-05 (Niedźwiedzia Cave)

The procedure was applied to develop a chronology for stalagmite NIED08-05 from Niedźwiedzia Cave, which lacks a robust U-Th chronology. Dating with U-Th was attempted and roughly confirms growth during most of the Holocene (present – 9000 yr BP). However, very large errors and numerous stratigraphic

inversions, related to low ^{230}Th and unknown initial $^{230}Th/^{232}Th$ ratios, prevent the construction of a reliable U-Th chronology for this stalagmite.

A continuous $a^{14}C$ decrease with increasing depth suggests that DCF and growth rate were stationary. Very stable $\delta^{13}C$ values (i.e., only a minor long-term trend) support this interpretation (Suppl. Fig. 1). However, the $a^{14}C$ values suggest that a hiatus exists and that growth rate is slightly different before and after the hiatus. The pre- and post-hiatus intervals were therefore considered separately, and two different growth models were constructed.

The younger (post-hiatus) interval was anchored to 2008 AD (the year of collection). The choice of the anchor point is justified by active dripping of the feeding stalactite and by the presence of the bomb spike in the top 0.4 mm of the stalagmite, both strongly suggesting recent growth. Additionally, the top ln ($a^{14}C$) value lies within the dataset's 1σ boundary, suggesting no growth rate anomalies (as was the case for HS4, Suppl. Fig. 2). The model reached convergence after four iterations, yielding a calculated mean growth rate of 0.0132 ± 0.0012 mm yr^{-1} and a growth interval from 3,833 ± 330 yr BP until 2008 AD (Fig. 5). The mean modelled DCF for the post-hiatus interval is 10% (±4%), similar to the DCF calculated from the bomb spike (~14%).

No independent anchor points exist below the hiatus and the chronology for pre-hiatus growth was developed using the methodology outlined in section 5.3. After three iterations, the model reached convergence, resulting in a mean growth rate of 0.0227 ± 0.00054 mm yr^{-1} over this lower interval. The modelled ages suggest that stalagmite NIED08-05 began growing at 7,961 ± 1,354 yr BP and continued until 4,876 ± 1,354 yr BP, at which point growth stopped for ~1,000 years (Fig. 5). However, because of the large dating uncertainty in this interval, these ages should be considered as only qualitative.

Because ^{14}C sample powders were obtained at a resolution (every 5 mm) that prevents pinpointing the location of the hiatus, the high resolution LA-ICPMS Mg concentration profile was used to locate its exact depth. At 51.5 mm depth, a

gradual increase to very high Mg values within the two ^{14}C samples bracketing the hiatus and coinciding with its probable petrographic expression occurs. This is followed by a very abrupt return to lower values (Suppl. Fig. 1), strongly suggesting that the hiatus is located at 51.5 mm depth. This feature probably reflects decreased rainfall and elevated Mg concentrations derived from high prior calcite precipitation (PCP) or bedrock dissolution (Sherwin & Baldini, 2011; Stoll et al., 2012), followed by abrupt growth cessation. Once drip water flow resumed and/or the drip water was again supersaturated with respect to calcite, stalagmite growth re-initiated and calcite Mg concentrations abruptly returned to lower values. Therefore, the exact location of the hiatus was placed at the transition between the highest Mg/Ca point and the return to the baseline. We are aware of the fact that other prominent excursions in Mg/Ca, as well as petrographic layers, exist throughout the record, which could indicate the presence of more growth hiatuses. However, the fact that these excursions are not accompanied by substantial shifts in ^{14}C suggests that these potential hiatuses (if present) were very short lived, and do not have a significant impact on the final chronology.

7.Evaluation of the age model

The procedure presented here provides accurate ^{14}C-based chronologies for some stalagmites where U-Th dating is not possible. Stalagmites amenable to this dating method are characterised by: *i)* stationary DCF without long-term secular variability, ii) stationary growth rate, iii) measurable ^{14}C decay, iv) the presence of an 'anchor point' (an independent age estimate) determined by other means, *iii)* growth during the last ~50ka (the current ^{14}C detection limit). The model provides a mean growth rate for a stalagmite by finding the best fit through all available ^{14}C ages, so small-scale growth rate variability is not resolvable. Two problems arise from this: first, stalagmites that experienced substantial growth rate shifts will have larger chronological uncertainty, potentially impeding the convergence of the iterative process, especially in the case of young stalagmites (i.e., where little ^{14}C-decay has occurred). However, a sufficiently high-resolution ^{14}C dataset could detect and model a growth rate change if the shift was large enough and occurred over a long time period. To test this, we produced a

synthetic dataset of a 192 mm long stalagmite where a substantial growth rate change occurs at 77.5 mm depth (0.0613 to 0.0133 mm yr^{-1}) and DCF varies between 12 and 16%. The ln ($a^{14}C$)-depth relationship highlights the growth rate change in the synthetic dataset (Fig. 6), illustrating that pronounced growth rate changes are detectable using raw ^{14}C data, and that, conversely, the model can confirm stationary growth rates (e.g., as in NIED08-05). Future refinements to the model could be made to fit the sections individually.

Additionally, and probably more importantly, the anchor point used in the model ultimately affects chronological accuracy. If the anchor point lies in an interval where the growth rate deviates considerably from its mean value, the resulting chronology will over- or under-estimate actual ages. Anchor selection and evaluation of the ^{14}C data is therefore crucial. As shown for stalagmite HS4, apparently small deviations of ln ($a^{14}C$) data can result in substantial offset of the final chronology, if not considered. Careful evaluation of potential anchor points with respect to their representativity of the entire dataset prior to the modelling procedure is therefore essential (Suppl. Fig. 2), and can help identify the best possible option in cases where multiple anchor points are available.

The ^{14}C data also highlight longer growth hiatuses, which complicate chronological development for older (pre-hiatus) intervals and introduce very large uncertainties. In the case of NIED08-05, mean pre-hiatus uncertainty is ± 1,354 years, essentially providing no chronological control except for a qualitative indication of the general growth interval (i.e., the early Holocene). Therefore, although the technique produces accurate chronologies for stalagmite growth periods with independent anchor points, intervals below hiatuses are currently problematic, and cannot be resolved quantitatively without an additional independent anchor point (e.g. one accurate U-Th age). Other geochemical information (e.g., Mg or $\delta^{13}C$) might provide useful constraints on DCF independent of an anchor point, greatly reducing dating uncertainties below hiatuses.

As high precision ^{14}C analysis requires much smaller sample sizes than U-Th (especially for young samples), a combination of high-resolution ^{14}C measurements and low-resolution U-Th measurements could provide a powerful tool to develop precise chronologies that have the advantage of high spatiotemporal resolution. This would allow determination of multiple anchor points for the procedure, providing more robust chronologies. Although U-Th remains the method of choice for high-precision dating of stalagmites, such a combined method could provide a powerful additional tool for dating Holocene stalagmites.

8.Refining the model: the potential for independent DCF estimation

Several studies illustrate that vegetation, soil, and hydrological conditions modulate DCF (Genty et al., 2001; Griffiths et al., 2012; Noronha et al., 2014; Oster et al., 2010; Rudzka-Phillips et al., 2013; Rudzka et al., 2011). Griffiths et al. (2012) found strong similarities between DCF and both Mg/Ca and $\delta^{13}C$ values in an Indonesian stalagmite from Liang Luar cave. Mg/Ca and $\delta^{13}C$ reflect karst hydrological conditions and general hydroclimate (Johnson et al. 2006; Partin et al. 2013; Stoll et al. 2012; Ridley et al. 2015), with drier conditions favouring higher $\delta^{13}C$ and Mg/Ca values because of lower soil bioproductivity, increased bedrock dissolution, enhanced degassing, and PCP (Johnson et al. 2006; Griffiths et al. 2012; Tremaine & Froelich 2013). For Liang Luar cave and several other sites, low recharge during dry periods promotes open system conditions (i.e., where water is in contact with an unlimited reservoir of soil CO_2) within the karst, allowing drip water dissolved inorganic carbon (DIC) to re-equilibrate with soil CO_2 and consequently lowering DCF. Conversely, closed system conditions associated with wetter periods promote higher DCF due to 'waterlogging' of the karst leading to reduced exchange between drip water and soil air (Fohlmeister et al., 2010; Griffiths et al., 2012).

Published Mg/Ca and $\delta^{13}C$ data from individual stalagmites often co-vary, implying hydrological control on both parameters (Fig. 7). Independent DCF estimation is theoretically possible on such stalagmites, due to the link between Mg/Ca, $\delta^{13}C$, and DCF. Data from stalagmite HS4 (Heshang cave, China) (Hu et al.,

2008; Liu et al., 2013; Noronha et al., 2014) were used to investigate this possibility. Because the original $\delta^{13}C$, Mg/Ca, and DCF were all sampled individually and at different depths, the datasets were resampled and smoothed to bring all parameters on the same timescale and reduce sampling bias. $\delta^{13}C$ and Mg/Ca are significantly correlated (r^2=0.68), and smoothing markedly improves the correlation (r^2=0.91, $p<0.001$). DCF and $\delta^{13}C$ are weakly correlated (r^2=0.13 for the original data; r^2=0.29, $p<0.001$, for smoothed data), and similarly DCF and Mg/Ca (r^2=0.21, for the original data; r^2=0.37, $p<0.001$, for smoothed data). Higher (lower) DCF values correspond to lower (higher) Mg/Ca and $\delta^{13}C$ values (Fig. 8). However, other factors such as contributions from the soil/vegetation system must drive a significant portion of the signal, impacting both $\delta^{13}C$ and DCF (Fohlmeister et al., 2011; Oster et al., 2010).

Considering only karst processes, the distance of a coupled Mg/Ca-$\delta^{13}C$ measurement from the point of initial DIC (before the start of limestone dissolution) should reflect DCF (Fig. 8). When applied to the HS4 dataset, this approach estimates DCF moderately well, although the amplitude of variation in the modelled results is much lower than measured, due to the smoothing of the $\delta^{13}C$ and Mg/Ca datasets (Suppl. Fig. 3). However, DCF varies considerably depending on cave and climatic settings (Genty et al. 1999), so that DCF from a single stalagmite (e.g., HS4) cannot be used to calibrate samples from other locations. Available published data suggest that very different and sample-specific relationships between DCF and $\delta^{13}C$ exist, and no clear pattern related to climate or cave settings is apparent (Suppl. Fig. 4). However, many of the available datasets are limited in size, and the relationships presented are not statistically significant.

These results illustrate that constraining DCF via Mg/Ca, and $\delta^{13}C$ data is potentially attainable, but the underlying processes and the interdependencies between parameters remains elusive. The lack of available data at sufficiently high resolution and in many cases sampling bias, such as not measuring all proxies on the same aliquot of powder, contribute to the uncertainty. Although

593 the paucity of robust datasets precludes reaching any firm conclusions with
594 respect to these observations, our work and previous studies on DCF and soil-
595 cave carbon transfer (e.g. Genty et al., 2001; Rudzka et al., 2011; Rudzka-Phillips
596 et al., 2013) suggest that climate does influence DCF. Tropical sites where
597 temperature is high throughout the year but rainfall is very seasonal (e.g., Liang
598 Luar cave) might produce different DCF responses than temperate sites where
599 both rainfall and temperature may vary seasonally (e.g., Niedźwiedzia cave). It is
600 likely that specific climate conditions at a cave site result in a continuum of
601 systems between tropical and temperate end members, resulting in different
602 DCF-$\delta^{13}C$ relationships.
603
604 9.Correcting the chronology for DCF variations
605 Our model estimates DCF, which can help adjust the final chronology for subtle
606 offsets from the constant growth trend. The residual DCF (i.e., the deviation of
607 each calculated DCF data point from the mean DCF) is used to calculate the
608 correction in years for each data point (using the modeled ages). These
609 corrections are applied to the modelled chronology, resulting in an "DCF
610 corrected" chronology that is compatible with existing chronology development
611 software (e.g., COPRA (Breitenbach et al., 2012), StalAge (Scholz and Hoffmann,
612 2011)). Dating uncertainty is comprised by the modelling uncertainty plus the
613 DCF estimation error. Applying this correction to the modelled HS4 chronology
614 reproduces long-term trends apparent in the U-Th based chronology (Fig. 9a and
615 b). The correction does introduce some age reversals, particularly in the older
616 and highly resolved intervals of HS4; the chronology was therefore
617 downsampled to remove inversions prior to COPRA treatment.
618
619 The model can reliably estimate DCF (Fig. 4c), suggesting that a common process
620 controls both growth rate and DCF, possibly recharge conditions. Growth rate
621 and DCF in stalagmite HS4 appear weakly anti-correlated ($r^2 = 0.14$), and it is
622 possible that elevated rainfall at the Heshang cave site encourages closed-system
623 conditions and increased DCF, while simultaneously reducing the DIC of the
624 percolation water and stalagmite growth rate. We emphasise that although the
625 model appears to yield reasonable DCF estimates, the reasons why DCF is linked

to growth rate are unclear. Furthermore, although the DCF correction appears to work for HS4, its applicability to non-monsoonal sites where temperature may play a larger role in DCF determination is unknown. We present a provisional DCF-corrected chronology for NIED08-05, but emphasise that whether the relationship observed in HS4 is transferrable to NIED08-05 is not known. Despite these uncertainties, the DCF corrected NIED08-05 chronology shows only very minor differences to the uncorrected chronology, consistent with the stationary $\delta^{13}C$ and the stable, slow growth rate of the sample.

10.Summary and conclusions

This study describes a novel approach to develop chronologies for stalagmites using ^{14}C. The model introduced estimates the average growth rate of a stalagmite from ^{14}C ages, taking into account past variations in atmospheric ^{14}C, and anchors the chronology to a point of known age. The model does not require DCF estimation, which is advantageous considered that DCF remains an enigmatic parameter with respect to its influencing factors. Application of the model on a U-Th dated stalagmite, a synthetic dataset, and a stalagmite without a U-Th chronology, demonstrates that this method produces reliable chronologies provided the sample's long-term growth rate was regular and DCF was stationary. The choice of the anchor point is crucial and ultimately defines chronological accuracy. This currently leads to two main issues:

- Deviations from the long-term growth rate close to the anchor point will lead to chronological bias, as illustrated in the case of stalagmite HS4. However, measured ^{14}C ages, particularly when highly resolved, can reveal potentially anomalous growth rate shifts, and justify anchor point selection.

- Depositional hiatuses result in very large chronological uncertainty in the pre-hiatus interval of stalagmite growth, if no independent anchor point exists. The magnitude of the error (>1000 yr) results in virtually no chronological control for those intervals, and provides only qualitative information.

Future work may overcome these limitations, possibly by coupling the approach described here with other lines of geochemical information (e.g., Mg/Ca and $\delta^{13}C$ data) that may provide independent constrains on DCF. Although still being less precise than dating using the U-Th method, this current model as presented provides chronologies for stalagmites meeting certain criteria, and represents a useful alternative in cases where more established techniques are not applicable, or in combination with U-Th dating.

Acknowledgement:

The authors gratefully acknowledge help from the LIP staff members, especially Lukas Wacker during sample preparation and measurement. Dr Louise Thomas and Prof. Peter van Calsteren are thanked for their efforts with the U-Th dating of NIED08-05. Dr Wolfgang Müller is thanked for the LA-ICPMS aspects of the research. Dr Alexandra Noronha is thanked for useful review input to the manuscript. This research was supported by the European Research Council grant 240167 to JULB.

References:

Adkins, J.F., Carolin, S.A., Cobb, K.M., Subhas, A.V., Rider, A., Meckler, N., 2013. U-Series Dating of Tropical Stalagmites. Am. Geophys. Union.

Appleby, P.G., Oldfield, F., 1978. The calculation of lead-210 dates assuming a constant rate of supply of unsupported 210Pb to the sediment. Catena 5, 1–8. doi:10.1016/S0341-8162(78)80002-2

Baldini, J.U.L., McDermott, F., Baker, a., Baldini, L.M., Mattey, D.P., Railsback, L.B., 2005. Biomass effects on stalagmite growth and isotope ratios: A 20th century analogue from Wiltshire, England. Earth Planet. Sci. Lett. 240, 486–494. doi:10.1016/j.epsl.2005.09.022

Baskaran, M., Nix, J., Kuyper, C., Karunakara, N., 2014. Problems with the dating of sediment core using excess 210Pb in a freshwater system impacted by large scale watershed changes. J. Environ. Radioact. 138, 355–363. doi:10.1016/j.jenvrad.2014.07.006

Bieronski, J., Stefaniak, K., Hercman, H., Socha, P., Nadachowski, A., 2009. Palaeogeographic and palaeocological analysis of sediments of the Niedzwiedzia Cave in Kletno, in: Stefaniak, K., Tyc, A., Socha, P. (Eds.), Karst of the Czestochowa Upland and of the Eastern Sudetes: Paleoenvironments and Protection. Faculty of Earth Sciences University of Silesia, Zoological Institute University of Wroclaw, pp. 401–422.

697 Breitenbach, S.F.M., Rehfeld, K., Goswami, B., Baldini, J.U.L., Ridley, H.E., Kennett,
698 D.J., Prufer, K.M., Aquino, V. V., Asmerom, Y., Polyak, V.J., Cheng, H., Kurths, J.,
699 Marwan, N., 2012. Constructing proxy records from age models (COPRA).
700 Clim. Past 8, 1765–1779. doi:10.5194/cp-8-1765-2012

701 Broecker, W.S., Olson, E.A., Orr, P.C., 1960. Radiocarbon Measurements and
702 Annual Rings in Cave Formations. Nature 185, 93–94.
703 doi:10.1038/185093a0

704 Cheng, H., Edwards, R.L., Broecker, W.S., Denton, G.H., Kong, X., Wang, Y., Zhang,
705 R., Wang, X., 2009. Ice age terminations. Science 326, 248–252.
706 doi:10.1126/science.1177840

707 Cheng, H., Lawrence Edwards, R., Shen, C.C., Polyak, V.J., Asmerom, Y., Woodhead,
708 J., Hellstrom, J., Wang, Y., Kong, X., Spötl, C., Wang, X., Calvin Alexander, E.,
709 2013. Improvements in 230Th dating, 230Th and 234U half-life values, and
710 U-Th isotopic measurements by multi-collector inductively coupled plasma
711 mass spectrometry. Earth Planet. Sci. Lett. doi:10.1016/j.epsl.2013.04.006

712 Don, J., 1989. Jaskinia na tle ewolucji geologicznej Masywo Snieznika, in: Jahn, A.,
713 Kozlowski, S., Wiszniowska, T. (Eds.), Jaskinia Niedzwiedzia W Kletnie.
714 Badania I Udostepnianie. Ossolineum, Wroclaw-Warszawa-Krakow-Gdansk-
715 Lodz, pp. 58–79.

716 Dorale, J.A., Edwards, R.L., Alexander, Jr., E.C., Shen, C.-C., Richards, D.A., Cheng,
717 H., 2007. Uranium-series dating of speleothems: Current techniques, limits,
718 & applications, in: Sasowsky, I.R., Mylroie, J. (Eds.), Studies of Cave
719 Sediments: Physical and Chemical Records of Paleoclimate. Springer, pp.
720 177–197.

721 Drysdale, R., Zanchetta, G., Hellstrom, J., Maas, R., Fallick, A., Pickett, M.,
722 Cartwright, I., Piccini, L., 2006. Late Holocene drought responsible for the
723 collapse of Old World civilizations is recorded in an Italian cave flowstone.
724 Geology 34, 101–104. doi:10.1130/G22103.1

725 Edwards, R.L., Chen, J.H., Wasserburg, G.J., 1987. U-238-U-234-Th-230-Th-232
726 systematics and the precise measurement of time over the past 500,000
727 years. Earth Planet. Sci. Lett. 81, 175–192. doi:10.1016/0012-
728 821X(87)90154-3

729 Fairchild, I.J., Smith, C.L., Baker, A., Fuller, L., Spötl, C., Mattey, D., McDermott, F.,
730 2006. Modification and preservation of environmental signals in
731 speleothems. Earth-Science Rev. 75, 105–153.
732 doi:10.1016/j.earscirev.2005.08.003

733 Fohlmeister, J., Kromer, B., Mangini, A., 2011. The influence of soil organic matter
734 age spectrum on the reconstruction of atmospheric 14C levels via
735 stalagmites. Radiocarbon 53, 99–115.

736 Fohlmeister, J., Schröder-Ritzrau, A., Spötl, C., Frisia, S., Miorandi, R., Kromer, B.,
737 Mangini, A., 2010. The influences of hydrology on the radiogenic and stable
738 carbon isotope composition of cave drip water, Grotta di Ernesto (Italy).
739 Radiocarbon 52, 1529–1544.

740 Francois, R., Bacon, M.P., Suman, D.O., 1990. Thorium 230 profiling in deep-sea

741 sediments: high-resolution records of flux and dissolution of carbonate in
742 the equatorial Atlantic during the last 24'000 years. Paleoceanography 5,
743 761–787.

744 Gascoyne, M., 1992. Palaeoclimate determination from cave calcite deposits.
745 Quat. Sci. Rev. 11, 609–632. doi:10.1016/0277-3791(92)90074-I

746 Genty, D., Baker, A., Massault, M., Proctor, C., Gilmour, M., Pons-Branchu, E.,
747 Hamelin, B., 2001. Dead carbon in stalagmites: Carbonate bedrock
748 paleodissolution vs. ageing of soil organic matter. Implications for 13C
749 variations in speleotherms. Geochim. Cosmochim. Acta 65, 3443–3457.
750 doi:10.1016/S0016-7037(01)00697-4

751 Genty, D., Massault, M., 1999. Carbon transfer dynamics from bomb-14C and
752 d13C time series of a laminated stalagmite from SW France - Modelling and
753 comparison with other stalagmite records. Geochim. Cosmochim. Acta 63,
754 1537–1548. doi:10.1016/S0016-7037(99)00122-2

755 Genty, D., Massault, M., Gilmour, M., Baker, A., Verheyden, S., Kepens, E., 1999.
756 Calculations of past dead carbon proportion and variability by the
757 comparison of AMS 14C and TIMS U/Th ages on two Holocene stalagmites.
758 Radiocarbon 41, 251–270.

759 Genty, D., Vokal, B., Obelic, B., Massault, M., 1998. Bomb 14 C time history
760 recorded in two modern stalagmites — importance for soil organic matter
761 dynamics and bomb 14 C distribution over continents. Earth Planet. Sci.
762 Lett. 160, 795–809.

763 González-Lemos, S., Jiménez-Sánchez, M., Stoll, H.M., 2015. Sediment transport
764 during recent cave flooding events and characterization of speleothem
765 archives of past flooding. Geomorphology 228, 87–100.
766 doi:10.1016/j.geomorph.2014.08.029

767 Green, H., Woodhead, J., Hellstrom, J., Pickering, R., Drysdale, R., 2013. Re-
768 analysis of key evidence in the case for a hemispherically synchronous
769 response to the Younger Dryas climatic event. J. Quat. Sci. 28, 8–12.
770 doi:10.1002/jqs.2605

771 Griffiths, M.L., Drysdale, R.N., Gagan, M.K., Frisia, S., Zhao, J. xin, Ayliffe, L.K.,
772 Hantoro, W.S., Hellstrom, J.C., Fischer, M.J., Feng, Y.X., Suwargadi, B.W., 2010.
773 Evidence for Holocene changes in Australian-Indonesian monsoon rainfall
774 from stalagmite trace element and stable isotope ratios. Earth Planet. Sci.
775 Lett. 292, 27–38. doi:10.1016/j.epsl.2010.01.002

776 Griffiths, M.L., Fohlmeister, J., Drysdale, R.N., Hua, Q., Johnson, K.R., Hellstrom,
777 J.C., Gagan, M.K., Zhao, J.X., 2012. Hydrological control of the dead carbon
778 fraction in a Holocene tropical speleothem. Quat. Geochronol. 14, 81–93.
779 doi:10.1016/j.quageo.2012.04.001

780 Hendy, C.H., Wilson, a. T., 1968. Palaeoclimatic Data from Speleothems. Nature
781 219, 48–51. doi:10.1038/219048a0

782 Hodge, E., Mcdonald, J., Fischer, M., Redwood, D., Hua, Q., 2011. Using the 14C
783 bomb pulse to date young speleothems. Radiocarbon 53, 345–357.

784 Hoffmann, D.L., Beck, J.W., Richards, D. a., Smart, P.L., Singarayer, J.S., Ketchmark,
785 T., Hawkesworth, C.J., 2010. Towards radiocarbon calibration beyond 28 ka
786 using speleothems from the Bahamas. Earth Planet. Sci. Lett. 289, 1–10.
787 doi:10.1016/j.epsl.2009.10.004

788 Hoffmann, D.L., Prytulak, J., Richards, D. a., Elliott, T., Coath, C.D., Smart, P.L.,
789 Scholz, D., 2007. Procedures for accurate U and Th isotope measurements by
790 high precision MC-ICPMS. Int. J. Mass Spectrom. 264, 97–109.
791 doi:10.1016/j.ijms.2007.03.020

792 Holmgren, K., Lauritzen, S.-E., Possnert, G., 1994. 230Th/234U and 14C dating of
793 a late Pleistocene stalagmite in Lobatse II cave, Botswana. Quat. Geochronol.
794 13, 111–119.

795 Hu, C., Henderson, G.M., Huang, J., Xie, S., Sun, Y., Johnson, K.R., 2008.
796 Quantification of Holocene Asian monsoon rainfall from spatially separated
797 cave records. Earth Planet. Sci. Lett. 266, 221–232.
798 doi:10.1016/j.epsl.2007.10.015

799 Hua, Q., Barbetti, M., Rakowski, a Z., 2013. Atmospheric radiocarbon for the
800 period 1950-2010. Radiocarbon 55, 2059–2072.
801 doi:10.2458/azu_js_rc.v55i2.16177

802 Hua, Q., McDonald, J., Redwood, D., Drysdale, R., Lee, S., Fallon, S., Hellstrom, J.,
803 2012. Robust chronological reconstruction for young speleothems using
804 radiocarbon. Quat. Geochronol. 14, 67–80.
805 doi:10.1016/j.quageo.2012.04.017

806 Johnson, K.R., Hu, C., Belshaw, N.S., Henderson, G.M., 2006. Seasonal trace-
807 element and stable-isotope variations in a Chinese speleothem: The
808 potential for high-resolution paleomonsoon reconstruction. Earth Planet.
809 Sci. Lett. 244, 394–407. doi:10.1016/j.epsl.2006.01.064

810 Li, W.-X., Lundberg, J., Dickin, A.P., Ford, D.C., Schwarcz, H.P., McNutt, R., Williams,
811 D., 1989. High-precision mass spectrometric uranium-series dating of cave
812 deposits and implications for paleoclimate studies. Nature 339, 534–536.

813 Liu, Y.-H., Henderson, G.M., Hu, C.-Y., Mason, a. J., Charnley, N., Johnson, K.R., Xie,
814 S.-C., 2013. Links between the East Asian monsoon and North Atlantic
815 climate during the 8,200 year event. Nat. Geosci. 6, 117–120.
816 doi:10.1038/ngeo1708

817 Mattey, D., Lowry, D., Duffet, J., Fisher, R., Hodge, E., Frisia, S., 2008. A 53 year
818 seasonally resolved oxygen and carbon isotope record from a modern
819 Gibraltar speleothem: Reconstructed drip water and relationship to local
820 precipitation. Earth Planet. Sci. Lett. 269, 80–95.
821 doi:10.1016/j.epsl.2008.01.051

822 McDermott, F., Frisia, S., Huang, Y., Longinelli, A., Spiro, B., Heaton, T.H.E.,
823 Hawkesworth, C.J., Borsato, A., Keppens, E., Fairchild, I.J., Van der Borg, K.,
824 Verheyden, S., Selmo, E., 1999. Holocene climate variability in Europe:
825 Evidence from d18O, textural and extension-rate variations in three
826 speleothems. Quat. Sci. Rev. 18, 1021–1038. doi:10.1016/S0277-
827 3791(98)00107-3

828 Müller, W., Shelley, M., Miller, P., Broude, S., 2009. Initial performance metrics of
829 a new custom-designed ArF excimer LA-ICPMS system coupled to a two-
830 volume laser-ablation cell. J. Anal. At. Spectrom. 24, 209.
831 doi:10.1039/b805995k

832 Noronha, A.L., Johnson, K.R., Hu, C., Ruan, J., Southon, J.R., Ferguson, J.E., 2014.
833 Assessing influences on speleothem dead carbon variability over the
834 Holocene: Implications for speleothem-based radiocarbon calibration. Earth
835 Planet. Sci. Lett. 394, 20–29. doi:10.1016/j.epsl.2014.03.015

836 Oster, J.L., Montañez, I.P., Guilderson, T.P., Sharp, W.D., Banner, J.L., 2010.
837 Modeling speleothem δ13C variability in a central Sierra Nevada cave using
838 14C and 87Sr/86Sr. Geochim. Cosmochim. Acta 74, 5228–5242.
839 doi:10.1016/j.gca.2010.06.030

840 Partin, J.W., Cobb, K.M., Adkins, J.F., Tuen, A. a., Clark, B., 2013. Trace metal and
841 carbon isotopic variations in cave dripwater and stalagmite geochemistry
842 from northern Borneo. Geochemistry, Geophys. Geosystems 14, 3567–3585.
843 doi:10.1002/ggge.20215

844 Paton, C., Hellstrom, J., Paul, B., Woodhead, J., Hergt, J., 2011. Iolite: Freeware for
845 the visualisation and processing of mass spectrometric data. J. Anal. At.
846 Spectrom. 26, 2508. doi:10.1039/c1ja10172b

847 Pflitsch, A., Piasecki, J., 2003. Detection of an Airflow System in Niedzwiedzia
848 (Bear) cave, Kletno, Poland. J. cave karst Stud. 65, 160–173.

849 Piasecki, J., Sawinski, T., 2009. The Niedźwiedzia cave in the climatic
850 environment of the Kleśnica Valley (Śnieżnik Massif), in: Stefaniak, K., Tyc,
851 A., Socha, P. (Eds.), Karst of the Czestochowa Upland and of the Eastern
852 Sudetes: Paleoenvironments and Protection. Faculty of Earth Sciences
853 University of Silesia, Zoological Institute University of Wroclaw, pp. 423–
854 454.

855 Reimer, P., Bard, E., Bayliss, A., Beck, J.W., Blackwell, P.G., Bronk Ramsey, C., Buck,
856 C., Cheng, H., Edwards, R.L., Friedrich, M., Grootes, P.M., Guilderson, T.P.,
857 Haflidason, H., Hajdas, I., Hatté, C., Heaton, T.J., Hoffmann, D.L., Hogg, A.G.,
858 Hughen, K.A., Kaiser, K.F., Kromer, B., Manning, S.W., Niu, M., Reimer, R.W.,
859 Richards, D.A., Scott, E.M., Southon, J.R., Staff, R.A., Turney, C.S.M., van der
860 Plicht, J., 2013. IntCal13 and Marine13 Radiocarbon Age Calibration Curves
861 0–50,000 Years cal BP. Radiocarbon 55, 1869–1887.
862 doi:10.2458/azu_js_rc.55.16947

863 Ridley, H.E., Asmerom, Y., Baldini, J.U.L., Breitenbach, S.F.M., Aquino, V. V., Prufer,
864 K.M., Culleton, B.J., Polyak, V., Lechleitner, F. a., Kennett, D.J., Zhang, M.,
865 Marwan, N., Macpherson, C.G., Baldini, L.M., Xiao, T., Peterkin, J.L., Awe, J.,
866 Haug, G.H., 2015. Aerosol forcing of the position of the intertropical
867 convergence zone since ad 1550. Nat. Geosci. 8, 195–200.
868 doi:10.1038/ngeo2353

869 Rudzka-Phillips, D., McDermott, F., Jackson, a., Fleitmann, D., 2013. Inverse
870 modelling of the 14C bomb pulse in stalagmites to constrain the dynamics of
871 soil carbon cycling at selected European cave sites. Geochim. Cosmochim.
872 Acta 112, 32–51. doi:10.1016/j.gca.2013.02.032

873 Rudzka, D., McDermott, F., Baldini, L.M., Fleitmann, D., Moreno, A., Stoll, H., 2011.
874 The coupled d13C-radiocarbon systematics of three Late Glacial/early
875 Holocene speleothems; insights into soil and cave processes at climatic
876 transitions. Geochim. Cosmochim. Acta 75, 4321–4339.
877 doi:10.1016/j.gca.2011.05.022

878 Ruff, M., Wacker, L., Gäggeler, H.W., Suter, M., Synal, H.-A., Szidat, S., 2007. A gas
879 ion source for radiocarbon measurements at 200 kV. Radiocarbon 49, 307–
880 314.

881 Scholz, D., Frisia, S., Borsato, A., Spötl, C., Fohlmeister, J., Mudelsee, M., Miorandi,
882 R., Mangini, A., 2012. Holocene climate variability in north-eastern Italy:
883 Potential influence of the NAO and solar activity recorded by speleothem
884 data. Clim. Past 8, 1367–1383. doi:10.5194/cp-8-1367-2012

885 Scholz, D., Hoffmann, D.L., 2011. StalAge - An algorithm designed for construction
886 of speleothem age models. Quat. Geochronol. 6, 369–382.
887 doi:10.1016/j.quageo.2011.02.002

888 Sherwin, C.M., Baldini, J.U.L., 2011. Cave air and hydrological controls on prior
889 calcite precipitation and stalagmite growth rates: Implications for
890 palaeoclimate reconstructions using speleothems. Geochim. Cosmochim.
891 Acta 75, 3915–3929. doi:10.1016/j.gca.2011.04.020

892 Southon, J., Noronha, A.L., Cheng, H., Edwards, R.L., Wang, Y., 2012. A high-
893 resolution record of atmospheric 14C based on Hulu Cave speleothem H82.
894 Quat. Sci. Rev. 33, 32–41. doi:10.1016/j.quascirev.2011.11.022

895 Stoll, H.M., Müller, W., Prieto, M., 2012. I-STAL, a model for interpretation of
896 Mg/Ca, Sr/Ca and Ba/Ca variations in speleothems and its forward and
897 inverse application on seasonal to millennial scales. Geochemistry, Geophys.
898 Geosystems 13, 1–27. doi:10.1029/2012GC004183

899 Street, F.A., Grove, A.T., 1979. Global Maps of Lake-Level Fluctuations since
900 30'000 yr BP. Quat. Res. 12, 83–118.

901 Suess, H.E., 1980. The Radiocarbon Record in Tree Rings of the Last 8000 Years.
902 Radiocarbon 22, 200–209.

903 Synal, H.A., Stocker, M., Suter, M., 2007. MICADAS: A new compact radiocarbon
904 AMS system. Nucl. Instruments Methods Phys. Res. B 259, 7–13.
905 doi:10.1016/j.nimb.2007.01.138

906 Tremaine, D.M., Froelich, P.N., 2013. Speleothem trace element signatures: A
907 hydrologic geochemical study of modern cave dripwaters and farmed
908 calcite. Geochim. Cosmochim. Acta 121, 522–545.
909 doi:10.1016/j.gca.2013.07.026

910 Urban, J., Margielewski, W., Hercman, H., Zak, K., Zernitska, V., Pawlak, J.,
911 Schejbal-Chwastek, M., 2015. Relief-induced soil zones at the Cretaceous
912 sandstone-mudstone contact in the Stolowe Mountains, SW Poland.
913 Zeitschrift für Geomorphol. 59, 183–208. doi:10.1127/zfg

914 van Calsteren, P., Thomas, L., 2006. Uranium-series dating applications in natural
915 environmental science. Earth-Science Rev. 75, 155–175.

doi:10.1016/j.earscirev.2005.09.001

Verheyden, S., Keppens, E., Fairchild, I.J., McDermott, F., Weis, D., 2000. Mg, Sr and Sr isotope geochemistry of a Belgian Holocene speleothem: Implications for paleoclimate reconstructions. Chem. Geol. 169, 131–144. doi:10.1016/S0009-2541(00)00299-0

Wacker, L., Němec, M., Bourquin, J., 2010. A revolutionary graphitisation system: Fully automated, compact and simple. Nucl. Instruments Methods Phys. Res. B 268, 931–934. doi:10.1016/j.nimb.2009.10.067

Wang, Y.J., Cheng, H., Edwards, R.L., An, Z.S., Wu, J.Y., Shen, C.C., Dorale, J.A., 2001. A high-resolution absolute-dated late Pleistocene Monsoon record from Hulu Cave, China. Science 294, 2345–2348. doi:10.1126/science.1064618

Wigley, T.M.L., 1975. Carbon 14 dating of groundwater from closed and open systems. Water Resour. Res. 11, 324. doi:10.1029/WR011i002p00324

Figure captions:

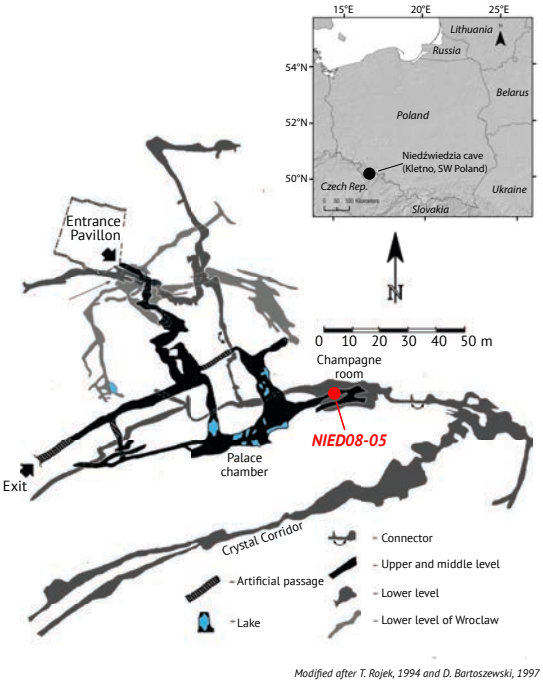

Figure 1: Map of Niedźwiedzia Cave and location of the cave in SW Poland (insert). The stalagmite NIED08-05 sampling location is indicated in red.

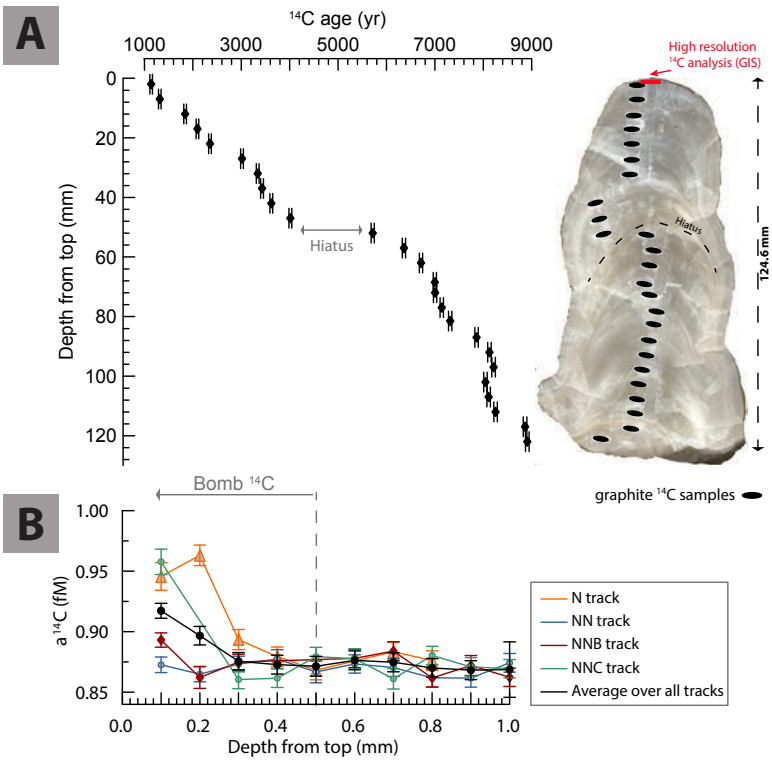

Figure 2: Results of the ^{14}C analysis on stalagmite NIED08-05. A: ^{14}C ages vs. depth from graphite analysis are shown in black; error bars denote 1σ errors. A scan of the stalagmite is shown on the far right, including indication of the sampling locations for ^{14}C and the location of the hiatus. B: results of high-resolution GIS measurements for ^{14}C across the top 1mm of stalagmite NIED08-05. Four different tracks were milled and analysed (shown in different colors and symbols), the average of all tracks is shown in black. Three of four profiles show a significant increase in a^{14}C in the top 0.5 mm, indicating the presence of bomb carbon and confirming recent growth of NIED08-05.

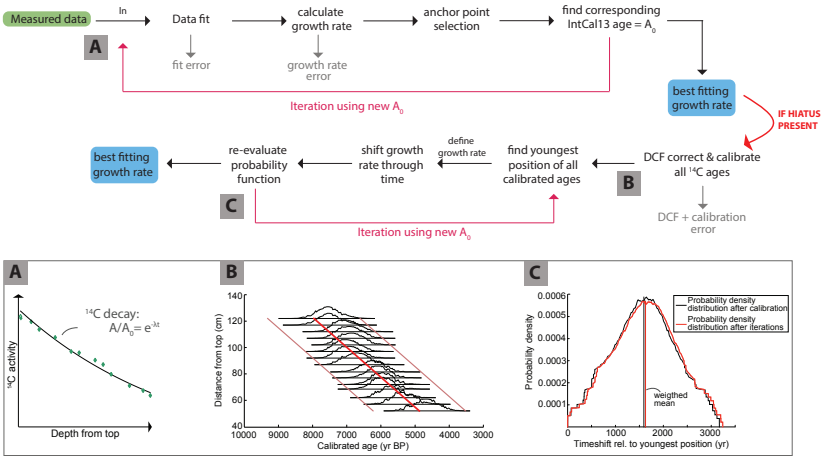

Figure 3: Flowchart illustrating the modelling steps in MATLAB for the construction of chronologies using ^{14}C. Small figures show some key steps in the modelling procedure. A) Conceptual figure illustrating the exponential decay pattern in measured ^{14}C data, a prerequisite for the successful construction of an age model. B) Calibration of pre-hiatus ages (when no independent anchor point is available). The growth rate line (red line) is positioned at the

youngest of all calibrated ages and then shifted through time until the best fit (i.e. point with highest probability for all ages) is found. 95% confidence intervals from calibration and DCF estimation are shown in light pink. C) While shifting the line through the probabilities, a new probability density distribution is established with respect to the youngest position, which reaches convergence after a few iterations of the model. The weighted mean (red line) of the probability density distribution is determined and used to find the best placement of the growth rate.

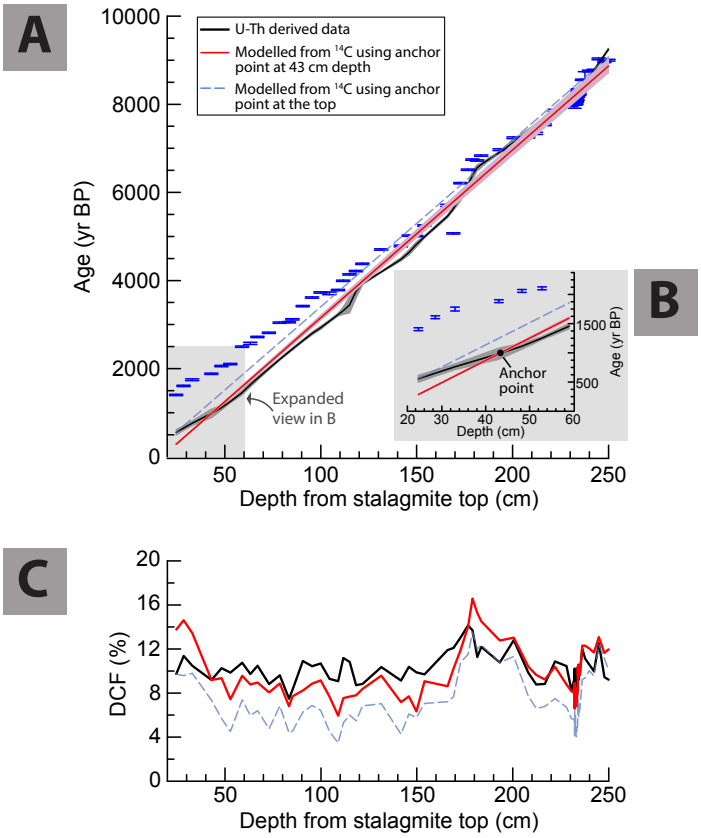

Figure 4: Modelling results for stalagmite HS4 from Heshang Cave, China. A: published age-depth relationship derived from the U-Th age model (black line), with 95% confidence bounds in grey (Hu et al., 2008; Noronha et al., 2014). Blue symbols show the measured, uncorrected and uncalibrated ^{14}C ages (Noronha et al., 2014). The red line indicates the age model derived from ^{14}C using the anchor point at 43 cm from top, with 95% confidence interval (this study). The dashed blue line is the modelled growth rate that would result if the anchor point was placed at the 24.6 cm from top (beginning of the ^{14}C dataset), where the actual growth rate deviates from the long-term mean (and ^{14}C ages are anomalous). This anchor point would result in a less accurate chronology, due to the bias from the ^{14}C ages. B: Expanded view of the top of the HS4 age model. The anchor point (fourth ^{14}C age, 43 cm from top) is indicated. C: DCF vs. depth plot. The black line indicates DCF derived from U-Th ages, the red line shows the DCF derived from our model anchored at 43 cm from top, and the blue dashed line is the modelled DCF using the anchor point at 24.6 cm from top.

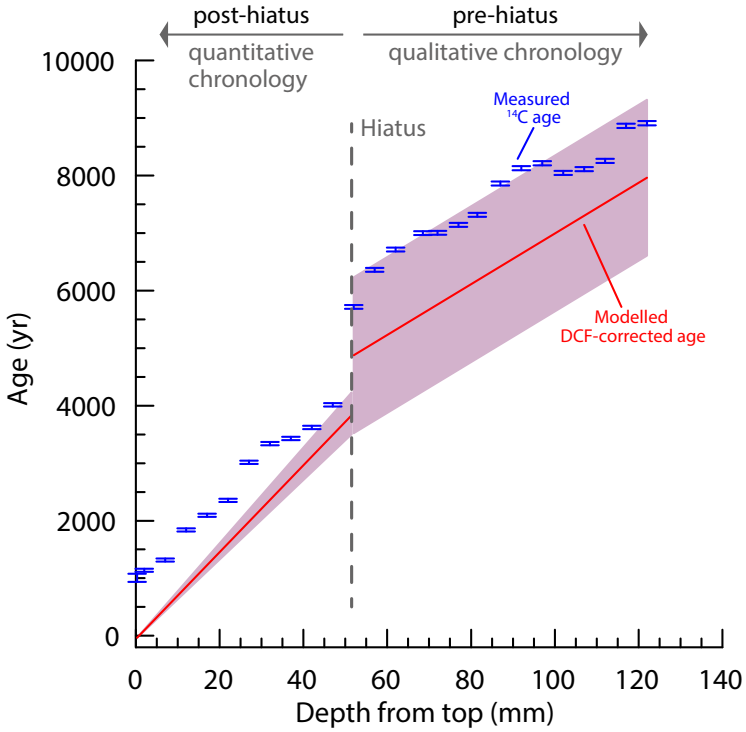

Figure 5: Chronology developed for stalagmite NIED08-05 from Niedźwiedzia Cave, Poland. Blue symbols show the measured ^{14}C ages (25 from graphite AMS analysis and one additional from GIS analysis averaging all measurements taken at 0.3 mm from top), and the anchor point used (2008 = year of collection). The red line indicates the best fitting growth rate derived from the presented model, with 95% confidence intervals. The depositional hiatus at 51.5 mm depth is marked by the grey dashed line. Very large age uncertainties in the pre-hiatus interval (due to the lack of an independent anchor point), result in this being only a qualitative chronology. It is also apparent that the uncertainty estimates for the pre-hiatus chronology are conservative, since most measured ^{14}C ages are younger than the maximum error. This problem could be solved by applying a stalagmite-specific threshold for the uncertainty, so that the resulting modelled chronology is younger than the measured ^{14}C ages (not shown).

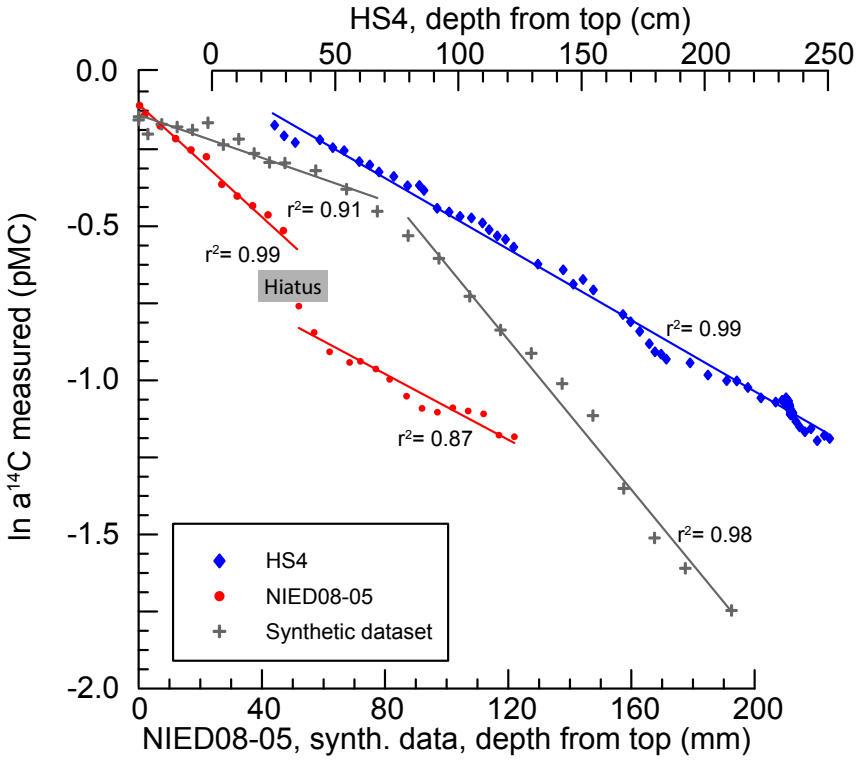

Figure 6: ln ($a^{14}C$)-depth relationships for stalagmite HS4 (blue diamonds), NIED08-05 (red squares) and a synthetic dataset showing a large and prolonged change in growth rate (grey crosses). The change in growth rate is clearly visible as a change in the slope of the synthetic dataset. This shows that major changes in growth rate can be detected in stalagmites with the procedure described in this study, and corroborates our assumption that NIED08-05 experienced relatively constant growth rates and is a suitable sample for the method described in this study.

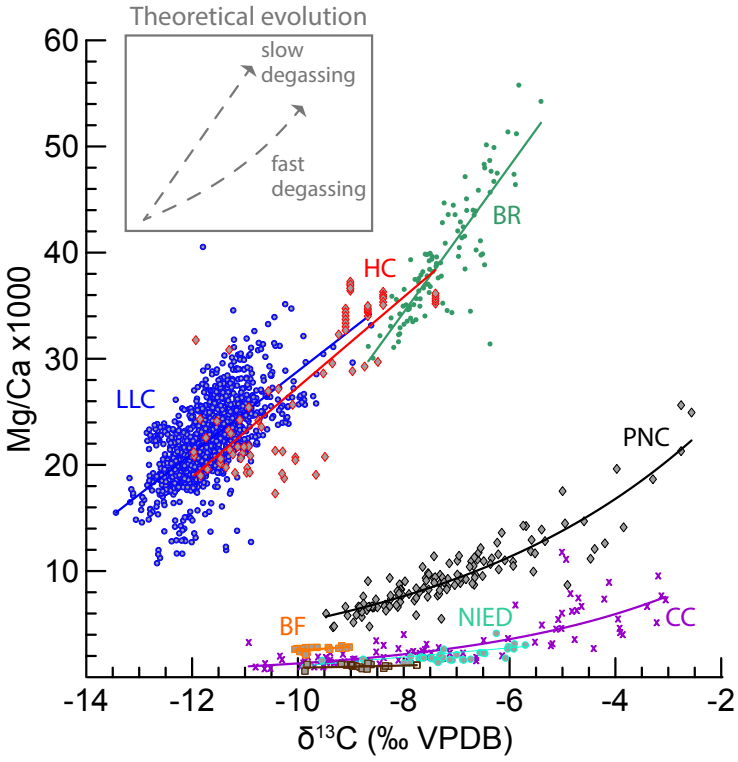

Figure 7: Compilation of Mg/Ca vs. $\delta^{13}C$ relationship for published stalagmite datasets from different cave systems. Abbreviations indicate the cave system: NIED- stalagmite NIED08-05, Niedźwiedzia cave, Poland, (this study); CC – Stalagmite CC-Bil, Crag cave, Ireland (McDermott et al., 1999); PNC – stalagmite PN95, Pere Noel cave, France (Verheyden et al., 2000); BF – Brown's Folly mine, England (Baldini et al., 2005); BR – flowstone RL-4, Buca della Renella, Italy (Drysdale et al., 2006); HC – stalagmite HS4, Heshang cave, China (Hu et al., 2008; Liu et al., 2013); LLC – stalagmite LR06-B1, Liang Luar cave, Indonesia (Griffiths et al., 2010). The regression lines showing the best fit are shown for each stalagmite, highlighting different Mg/Ca vs. $\delta^{13}C$ relationships depending on dripwater degassing rate, as described by Johnson et al. (2006).

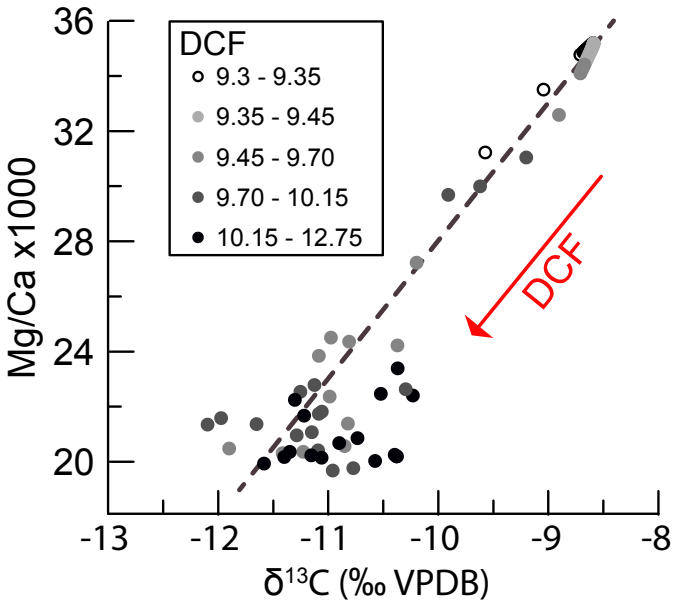

Figure 8: Relationships between $\delta^{13}C$, Mg/Ca and DCF in stalagmite HS4 from Heshang cave, China (Hu et al., 2008; Liu et al., 2013; Noronha et al., 2014). DCF decreases with increasing $\delta^{13}C$ and Mg/Ca, and could theoretically be quantified this way.

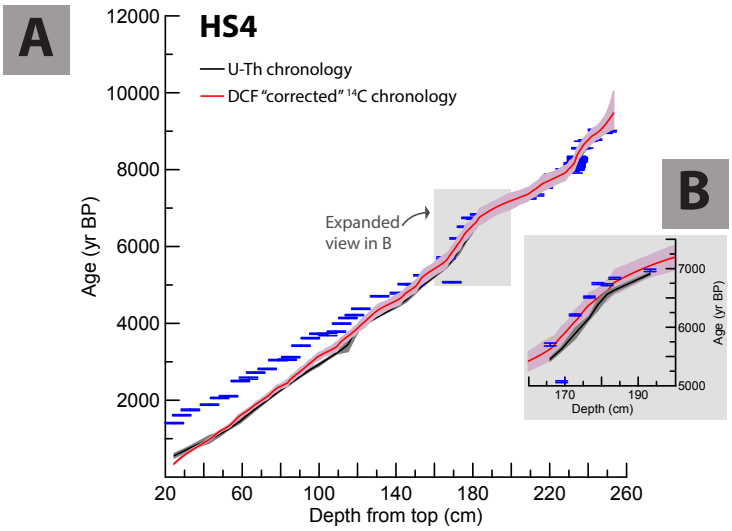

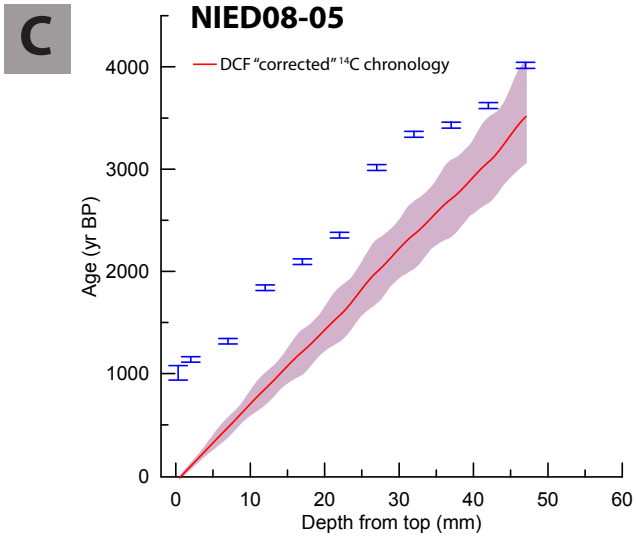

Figure 9: A) Offset corrected chronology for stalagmite HS4. Measured ^{14}C ages (blue) are compared to the U-Th chronology (black) and to the final corrected ^{14}C-derived chronology (red, uncertainty in pink). B) Detail of the HS4 chronology. C) Offset corrected chronology for stalagmite NIED08-05. Measured ^{14}C ages (blue) and final corrected ^{14}C-derived chronology (red, uncertainty in pink) are shown.

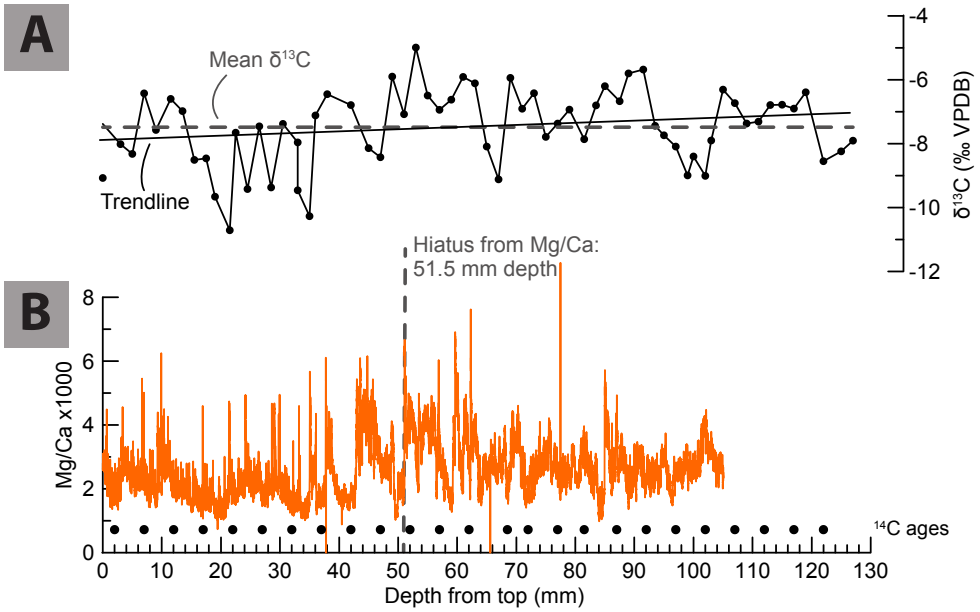

Suppl. Figure 1: A) $\delta^{13}C$ record for stalagmite NIED08-05. The dashed grey line indicates mean $\delta^{13}C$, the black line is the linear trendline of the dataset. Variation in $\delta^{13}C$ is relatively small (average: -7.48‰, σ: 1.17), and there is only a negligible long-term trend in the dataset, corroborating the assumption that variations in DCF were small as well. B) High resolution laser ablation Mg/Ca record for NIED08-05. Black dots indicate the position of ^{14}C ages. The dashed grey line shows the location of the hiatus at the local maximum Mg/Ca value. The gradual increase in Mg/Ca, followed by a sharp decrease back to baseline values is interpreted as increasingly dry conditions and enhanced PCP, followed by a growth stop until water started flowing again (with lower Mg/Ca). Therefore, the exact depth of the hiatus in NIED08-05 is placed at 51.5 mm from top.

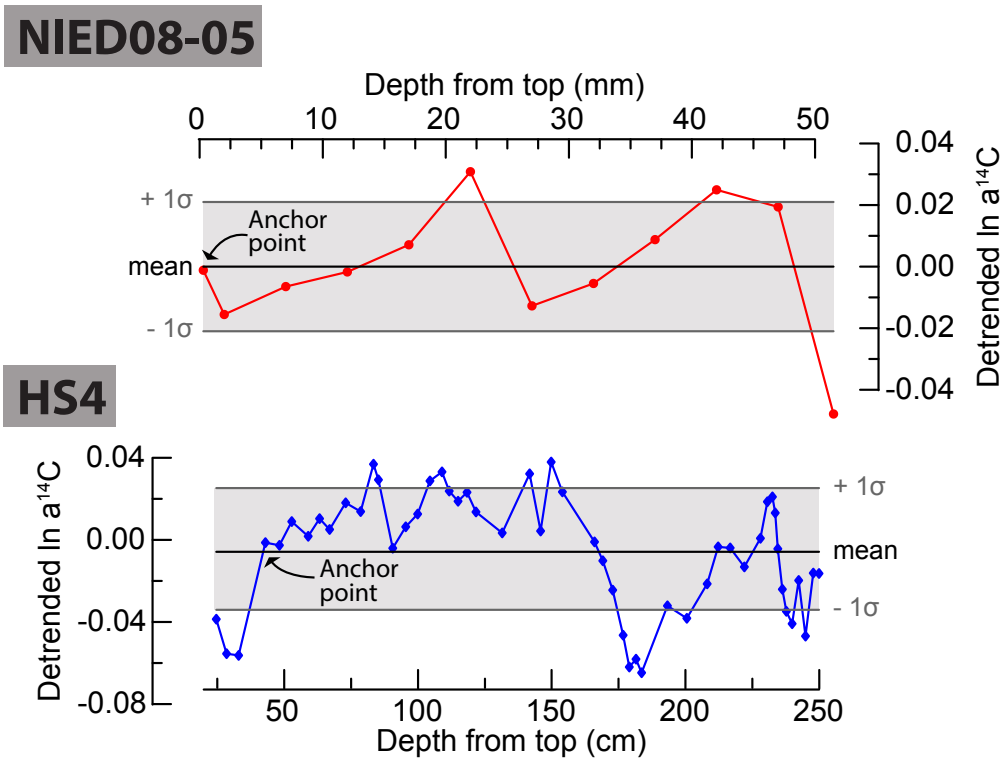

Suppl. Figure 2: Detrended ln ($a^{14}C$) data for stalagmites NIED08-05 and HS4 highlighting the importance of $a^{14}C$ values representative of the entire dataset at the anchor point. The top panel shows ln ($a^{14}C$) values for NIED08-05, including the mean and standard deviation. It is apparent that the top $a^{14}C$ value lies within the stalagmites 1σ boundary, justifying the choice of the anchor point at the top of the sample. In the lower panel, ln ($a^{14}C$) values, their mean and standard deviation for stalagmite HS4 are shown. The top three ln ($a^{14}C$) values are anomalous (outside of 1σ boundaries) and will therefore result in a chronological bias if used. The fourth ln ($a^{14}C$) value, however, is within the 1σ boundaries and can be used. This procedure should always be applied as a quality control for the chronology, and could greatly help in choosing the best anchor point if multiple possible anchors exist.

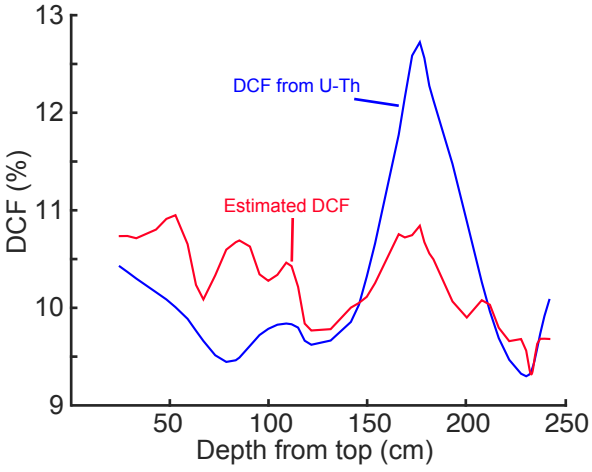

Suppl. Figure 3: Example of DCF modelling using Mg/Ca vs. $\delta^{13}C$ from stalagmite HS4, Heshang cave (Hu et al., 2008; Liu et al., 2013; Noronha et al., 2014), and re-applying the relationship on the same stalagmite. DCF calculated from U-Th chronology (blue line) and DCF estimated from the Mg/Ca vs. $\delta^{13}C$ relationship (red line) are shown. It is apparent that DCF variations can be modelled to a certain extent using this approach; however, the estimated DCF is strongly muted with respect to the actual DCF, due to the smoothing processes prior to the modelling. At present, this approach cannot be widely applied to stalagmites with unknown DCF, as the Mg/Ca vs. $\delta^{13}C$ – DCF relationship is cave-specific and difficult to quantify for the general case.

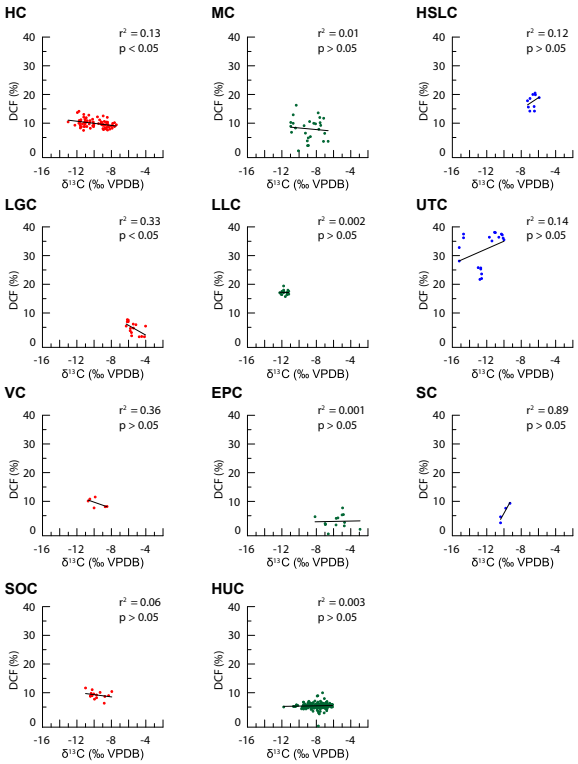

Suppl. Figure 4: Compilation of DCF vs. $\delta^{13}C$ relationships for published datasets from different caves. Positive correlation (red symbols): HC - stalagmite HS4, Heshang cave, China (Hu et al., 2008; Noronha et al., 2014); LGC - stalagmite GAR-01, La Garma cave, Spain (Rudzka et al., 2011); VC - stalagmite Vil-stm1, Villars cave, France (Genty et al. 1999); SOC - stalagmite So-1, Sofular cave, Turkey (Rudzka et al., 2011); Negative correlation (blue symbols): HSLC - stalagmites Han-stm1 and Han-stm5, Han-sur-Lesse cave, Belgium (Genty et al., 1999, 1998); UTC - stalagmites SU-2, SU-96-1, SU-96-7, Uamh-an-Tartair cave, Scotland (Genty et al., 2001); SC - stalagmite Sal-stm1, Salamandre cave, France (Genty et al., 2001); no correlation (green symbols): MC - stalagmite MC3, Moaning cave, California (Oster et al., 2010); LLC - stalagmite LR06-B1, Liang Luar cave, Indonesia (Griffiths et al., 2012); EPC - stalagmite Candela, El Pindal cave, Spain (Rudzka et al., 2011); HUC - stalagmite H-82, Hulu cave, China (Southon et al., 2012). High p-values for most of the correlations indicate their low significance, and therefore most of these relationships should be carefully evaluated. Datasets with more paired DCF-$\delta^{13}C$ measurements

could help improve our understanding of the governing factors for both proxies at specific sites and regionally/globally.

Table 1: Results from the high precision graphite AMS ^{14}C analysis for stalagmite NIED08-05.

Suppl. Table 1: Results from the high-resolution tracks of the top 1 mm of stalagmite NIED08-05. Analyses were conducted using a Gas Ion Source (GIS).